OPTOELECTRONICS AND ADVANCED MATERIALS – RAPID COMMUNICATIONS Vol. 3, No. 12, December 2009, p. 1299 - 1305

Revealing Fe_3O_4 nanoparticles aggregation dynamics using dynamic light scattering

D. CHICEA
Physics Dept., University Lucian Blaga of Sibiu, Dr. Ion Ratiu Str. 7-9, Sibiu, 550012, Romania

Fe_3O_4 nanoparticles in aqueous suspensions are not stable but aggregate, tremendously changing the spectra of their biomedical applications. A modified version of the Dynamic Light Scattering (DLS) setup experiment was used to monitor Fe_3O_4 nanoparticle aggregation in aqueous diluted suspension. The experimental setup and the data processing procedure is described in detail and the variation of the average aggregate diameter in time is presented in this work.

(Received November 06, 2009; accepted November 23, 2009)

Keywords: Fe_3O_4 nanoparticles, Static light scattering, Dynamic light scattering, Aggregates

1. Introduction

The heat transfer properties of a fluid were found to be considerably enhanced by adding a small amount of nanoparticles [1]. Such a suspension is currently named a nanofluid; it is a relatively new notion and was first mentioned by Choi in 1995 [2].

The nanoparticles have a continuous, irregular motion in nanofluids, which is the effect of several factors such as gravity, Brownian force, Archimede's force and friction force between fluid and the particles. The irregular nanoparticle motion in the fluid is the cause the remarkable enhancement of heat transfer properties of the nanofluids [3-6]. The irregular motion directly depends of the particle dimension therefore the particle size distribution dictates the rheological properties of the nanofluid.

In aqueous suspensions nanoparticles aggregate forming clusters of colloids with an isotropic shape, most probably caused by van der Waals attractions and weak magnetic attractions, which are both of the order of kT [7]. Cobalt nanoparticle are reported to aggregate in "bracelets" [8] which are distinct from the micrometer-sized rings created by rapidly evaporating films of dispersed nanoparticles, with regard to ring size (typically 5-12 particles and 50-100 nm in diameter). Reference [9] describes the preparation of robust micrometer size ring structures on mica surfaces. Ring shaped clusters of Co-PFS were patterned onto a thin gold film sputtered onto a silicon wafer that had been primed with a 5 nm layer of titanium as is reported in [10]. The clusters mentioned in [10] have diameters between 0.6 and 12 μm.

Nanoparticles are extensively considered for biomedical applications. As the living cells have dimensions of the order of microns and parts of the order of tens to hundreds of nanometers. Proteins are even smaller, having dimensions around 5 nanometers. With this in mind, it was easy to imagine that nanoparticle structured materials can be used in many ways to investigate, to modify living cells or to deliver certain substances or drugs to them without perturbing much the cells. Thus many practical applications were developed in the last years and are nicely presented in [11, 19] and in many other review papers, not cited here.

The shape of the nanoparticle is more often spherical but it can be cylindrical, plate-like and other shapes are possible. The size and size distribution are crucial in some cases, for example if penetration through a pore structure of a cellular membrane is required. Fe_3O_4 nanoparticles are of special interest for biomedical applications because they are not toxic and they can be metabolized by living organisms. They present a major inconvenient though, as they aggregate very fast in diluted aqueous suspension. As the human body fluids are aqueous solutions, transporting Fe_3O_4 nanoparticles through human blood to a tumor or to a specific organ using magnetic field might create serious problems as the nanoparticles aggregate during the transportation process through the blood vessels. Once big aggregates are present the rheological properties of the suspension are different and the suspension ceases to be a nanofluid any more.

Moreover, the size and size distribution are becoming extremely critical when quantum-sized effects are used to control material properties, therefore establishing a fast technique for measuring the size of the nanoparticles in suspension and for monitoring the aggregates formation rate is of interest.

The most accurate and also the most expensive technique uses to obtain a very high resolution image of an emulsion containing nanoparticles is the Transmission Electron Microscopy (TEM). The image is processes and the size distribution of the nanoparticles is the outcome. An example of using TEM is [13] but other hundreds of papers could be cited to have successfully used the technique to characterize the nanoparticle size distribution.

Other currently used methods for nanoparticle sizing are Atomic Force Microscopy (AFM), and ferromagnetic resonance (FMR), for magnetic nanoparticles. A comparison of the TEM with the AFM results is presented in [14]. The results in [13] reveal that the AFM measured

nanoparticle diameter appears to be reduced with 20% and the standard deviation appears to be increased with 15%. The differences in the diameter and in the standard deviation findings were associated with the AFM tip and the nanoparticle concentration on the substrate. The AFM technique, as the TEM, requires expensive equipment and a delicate, time consuming procedure to prepare the sample.

Another technique currently used in measuring the nanoparticle diameter is the X-ray powder diffraction. In the historical paper [15] it is stated that when subject to X ray beam "every crystalline substance gives a pattern; the same substance always gives the same pattern; and in a mixture of substances each produces its pattern independently of the others." The powder diffraction method is thus ideally suited for characterization and identification of polycrystalline phases. Today about 50,000 inorganic and 25,000 organic single component, crystalline phases, diffraction patterns have been collected and stored as standards. Moreover, the areas under the peak are related to the amount of each phase present in the sample. Most important for particle sizing, the Scherrer Equation, demonstrated in [16] is used frequently in X-Ray analysis, particularly powder diffraction, of materials. It relates the peak full width at half maximum of a specific phase of a material to the mean crystallite size of that material. This technique assumes that the nanoparticle size is the same as the size of the crystallite, which is not the case for magnetic nanofluids, which form clusters in certain conditions.

While the TEM above mentioned offers the best resolution, the sample requires specific preparation and can not be used for monitoring nanoparticle aggregation dynamics, simply because the very thin sample must be placed in vacuum. The X ray diffraction and the AFM techniques require a solid sample even if they are carried on in air at atmospheric pressure, but are slow, in respect of the time scale of nanoparticle aggregation, therefore they are not suited for investigating the aggregation process.

A lower cost alternative to these techniques and others not mentioned in this introductory part is based on the fact that the nanoparticles have a continuous, irregular motion in nanofluids, which is the effect of several factors such as Brownian force, Archimede's force, friction force between fluid and the particles and gravity, which becomes significant for micron sized particles but can be neglected for nanometer sized particles [9, 10, 17]. The method is called Dynamic Light Scattering (DLS) or Photon Correlation Spectroscopy (PCS) and the physical principles of the method are explained in [18 – 20] and other papers following them. Details on a modified version of DLS are presented in the next section together with the results on monitoring the aggregates dimension in time during a dilution process.

A different approach consists of recording the far field and performing a statistical analysis of the speckle image. The speckled image appears as a result of the interference of the wavelets scattered by the scattering centers (SC hereafter), each wavelet having a different phase and amplitude in each location of the interference field. The image changes in time as a consequence of the scattering centers complex movement of sedimentation and Brownian motion giving the aspect of "boiling speckles" [18, 19]. In papers like [20] an optical set-up is used to measure the correlation function in the near field, and reveals the near-field speckle dependence on the particles size. The work reported in [21, 22] uses a transmission optical set-up to measure the far field parameters like contrast and speckle size and reveals that speckle size and contrast are related to the average particle diameter. Reference [23] revealed a strong variation of the average speckle size and contrast with the concentration of the scattering centers. In a diluted aqueous suspension as aggregates are formed, both the concentration and the size of the scattering centers change in time, therefore these far field parameters, speckle size and contrast are not suited for monitoring the nanoparticle aggregation process.

Another system that contains scattering centers that aggregate and presents a particular interest in medicine is the human blood. For several decades the basic method of studying platelets aggregation has been the Born technique based on the increase in light transmission [24]. In the last years light scattering techniques were extensively used as alternative methods. The first idea was to use the information offered by the backward scattered light [25], technique that works well in the single scattering regime recording the light scattered backward by separate particles or their aggregates. Other development reported in the literature was applied to aggregation studies [26].

Another interesting procedure for monitoring the particle aggregation in human rich platelet plasma was resented in [27] and consists of monitoring the scattered light intensity variation at a certain small angle in 1.5 – 4 degrees range. The intensity variation is quantitatively modeled in terms of the two parameters first order Hill function to describe the platelets aggregation kinetics in [27].

An alternative approach used the time dependent forwardly scattered light recorded using a photodiode array in the angular range 1 - 15 degrees to describe the kinetics of platelet aggregation [28, 29]. Two angular domains with qualitatively different behaviors were clearly evidenced by the reported measurements. Below 6 degrees, the signal given by the photodiodes increases as the platelets turn into aggregates while the signal for higher angles 6 - 15 degrees decreases. The effect is explained by de dependence of the light scattering anisotropy by the size of the scattering object.

The next sections present the recipe used in nanofluid synthesis, the modified version of the DLS setup and data processing procedure with results.

2. Nanofluid preparation

The nanofluid preparation does not require any special equipment and was carried on at room temperature, which was 22 ^{o}C. The reagents used were: $FeCl_3 \cdot 6H2O$, $FeCl_2 \cdot 4H_2O$, ammonium hydroxide (NH_3[aq]) 25%, citric

acid ($C_6H_8O_7$), all produced by Merck, Darmstadt. All chemicals used were p.a. grade.

The solutions were prepared just before the measurements, in order to prevent their contamination with the atmospheric oxygen. The concentrations were 1M for $FeCl_3$, 2M for $FeCl_2$, 0.5 M for ammonium hydroxide and 25% for citric acid. 4mL of the 1M $FeCl_3$ solution and 1 mL of the 2M $FeCl_2$ solution were poured into a 150 mL beaker. While continuously stirring the iron chloride solution, 50 mL of the 0.5 M ammonium hydroxide were slowly added, dropwise, in such a way that the process lasted for 5 minutes. A black precipitate formed during the slow addition, the precipitate being magnetite ($Fe^{2+}Fe^{3+}{}_2O_4$). A strong magnet was placed under the beaker. It accelerated the precipitation of magnetite out of the solution, and the water become clear. Keeping the magnet on the bottom of the beaker, the excess water was decanted.

The magnetite was rinsed three times by adding deionized water, using the magnet to settle the magnetite, and discarding the clear water, to remove the excess ammonium hydroxide from the particles. A viscous fluid was the result.

At this stage of the synthesis procedure the nanofluid, which in this case is a ferrofluid, was stabilized. This was accomplished by adding 1 mL of the 25% citric acid and mixing the ferrofluid for 2 minutes. Overall the chemical reaction was [30]:

$$2FeCl_3 + FeCl_2 + 8NH_3 + 4H_2O \rightarrow Fe_3O_4 + 8NH_4Cl \quad (6)$$

The output was a viscous, dark brown fluid having the volume ratio of 33%. Details on nanofluid synthesis and rheological properties are presented in [30].

3. The modified dynamic light scattering technique (DLS)

Dynamic light scattering (DLS) is a well established technique for measuring particle size over a size range from nanometers to microns. As previously stated the light scattered by a suspension presents fluctuations [18, 19]. By placing a detector at a certain angle and recording the scattered light intensity a time series is recorded. As proved in [31, 32] the width of the autocorrelation function of the time series is proportional to the diffusion coefficient, which, on it's turn, depends of the particle diameter. This leads to a fast procedure for measuring the particle diameter. An improved version is described further on in this section.

The early experimental works [33, 34] and the later theoretical treatises [35 - 38] proved the assumption that the powerspectrum of the intensity of the light scattered by particles in suspension can be linked to the probability density function (hereafter PDF). This link between the PDF and the powerspectrum is a consequence of the translation of the relative motion of the scattering particles into phase differences of the scattered light. Thus spatial correlations are translated into phasecorrelations, which is manifested in the usage of the Wiener-Khintchine-Theorem, relating the power spectrum to the autocorrelation of a process. The phase correlations lead to fluctuations in the intensity of the scattered light recorded using a detector and a data acquisition system, in a typical experimental setup as presented in Fig. 1.

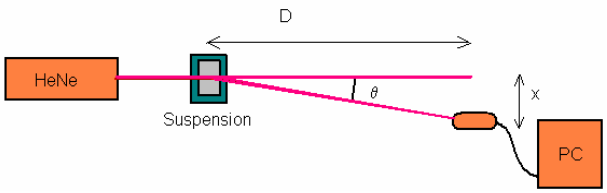

Fig. 1. A typical DLS experimental setup.

A sequence of a time series recorded for sample lm9-3 is presented in Fig. 2. By subtracting the average intensity from the recorded time series and calculating the square of the intensity we obtain the power time series. The Fourier transform of the power time series is the power spectrum. We can compare the spectrum calculated from the experimental data with the theoretically expected spectrum, namely the functional form of the Lorentzian line S(f) (1).

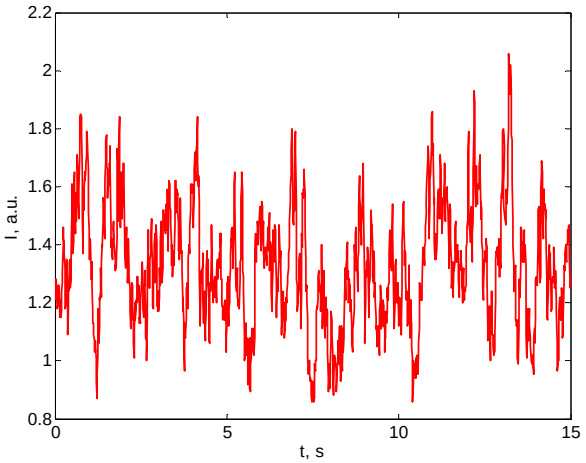

Fig. 2. A sequence of a time series recorded for sample lm9-3.

$$S(f) = a_0 \cdot \frac{a_1}{(2\pi f) + a^2_1} \quad (1)$$

The Lorentzian line S(f) has two free parameters a_0 and a_1 and is fit to the powerspectrum using a non-linear minimization procedure to minimize the distance between the data-set and the line. We notice that a_0 enters linearly, thus only performs a scaling of the function in the range, which translates into a shift in the logarithmic representation. The a_1 parameter enters nonlinearly into the function. Its effect in the log-log scaled plot can approximately be described as a shift along the frequency axis. The possibility to fit the whole function is advantageous compared to the alternative method described in [33, 34, 38] where the $f_{1/2}$ (the frequency

where half-maximal-height is reached) was measured, since it takes more datapoints into account, thus increasing the quality of the fit.

Once the fit is completed and the parameters are found, the diameter of the SCs can be assessed as the double of the radius R. The radius can be derived as a function of the fitted parameter a_1 and other known quantities using (2):

$$R = \frac{2k_B TK^2}{6\pi\eta a_1} \tag{2}$$

Where

$$K = \frac{4\pi n}{\lambda}\cdot\sin\left(\frac{\theta}{2}\right) \tag{3}$$

In (2) k_B is Boltzman's constant, T is the absolute temperature of the sample, η is the dynamic viscosity of the solvent. In (3) θ is the scattering angle, n is the refractive index of the scattering particles and λ is the wavelength of the laser radiation in vacuum.

The work described in this article was carried on using an experimental setup as described in Fig. 1. The wavelength was 633 nm, the light source was a He-Ne laser and the power was 2 mW. The DLS experiment was carried on at 20 ^oC. The cuvette-detector distance D was 0.615 m and x was 0.03 m making the scattering angle θ equal to 2^o 47' 34''. This is not typical for DLS where a bigger angle is chosen, usually 90^o. The reason for choosing such a small angle is to shift the rollover point in the Lorentzian line towards smaller a_1 values, hence smaller frequencies, where the noise is considerably smaller.

A 900 seconds time series was recorded using the experimental setup in Fig. 1 and the values of the parameters describes above. As the purpose of the experiment was to monitor the nanoparticle aggregation process, a program was used to slice the time series into chunks or slices of data, using the desired time interval for each data chunk or slice, which is given as an input parameter. We should note however that using a small time span for each data slice will apparently increase the accuracy of the monitoring process but will decrease the precision of the Lorentzian function (1) fit as the amount of data to be fitted is smaller. Increasing the time span for each data slice will increase the precision of the fit but will provide a poor information of the variation of the aggregates dimension in time. With this in mind, the time span of each time series slice was chosen to be 15 seconds.

Special care must be taken to start the recording simultaneously with the beginning of the dilution process and to produce a strong agitation and stirring of the aqueous suspension, otherwise the diffusion of the nanoparticles is slow compared with the time span of the experiment and the results might not be reproducible as different concentrations might occur in the beam area of the cuvette.

For the experiments described in this article a 10×10×40 mm quartz cuvete was used. First 0.01 ml concentrated nanofluid was introduced into a 5 ml syringe and after it 4.99 ml of deionised water was aspired in. At the time of deionised water aspiration the time series recording was started. The mixture was injected fast into the cuvette producing turbulences. Right after that a certain fluid quantity was aspired and injected back. The procedure of aspiring and injecting fast the suspension was repeated three times in order to obtain a homogeneous suspension. The amount of aspired fluid was small enough that the laser beam remained under the upper surface of the fluid at all times. Anyway, due to the turbulences produced by the aspiration procedure the velocity of the SCs was different from the velocity of the natural Brownian motion and this can lead to false DLS particle size. For this reason the first 7 seconds from the first slice of the time series was not processed as previously described.

Prior to the experiment the concentrated nanoparticle suspension was diluted in 25% citric acid, in order to prevent aggregation and a DLS time series was recorded. The time series was analysed using the procedure described above. The PSD (blue line) and the fitted Lorentzian line for the time series recorded on sample lm9-3 are presented in Fig. 3.

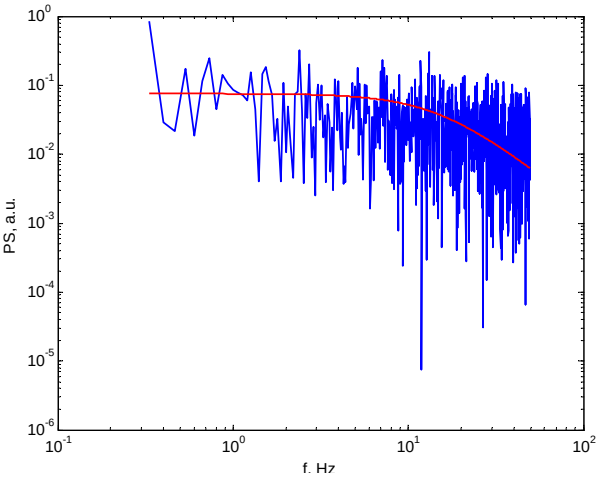

Fig. 3. The PSD (blue line) and the fitted Lorentzian line (smooth) for the time series recorded on nanofluid diluted in citric acid to prevent aggregation.

The parameters of the Lorentzian line found from the fit are: a_0=2.27 and a_1=30.00. Using (2) we found that the SCs have an average diameter of $18\cdot10^{-9}$ m. The PSD (blue line) and the fitted Lorentzian line for the first time series, allotted to time 7+4=11s are presented in Fig. 4. The parameters of the Lorentzian line that produce the best fit are: a_0=5.0034 and a_1=1.2615. Using (2) we found that the SCs have an average diameter of $418\cdot10^{-9}$ m, considerably bigger than the average diameter of the SCs measured in the concentrated suspension.

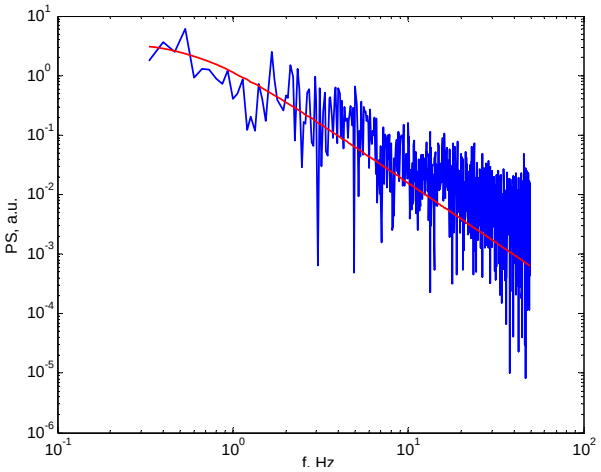

Fig. 4. The PSD (blue line) and the fitted Lorentzian line (smooth) for the time series slice allotted to time 11 s since the dilution was started on sample lm9-3.

The fitting procedure was repeated for all the consecutive time slices recorded during the experiment and the average diameter was calculated. The variation of the average diameter in time calculated using the modified version of the DLS particle sizing, as described above, is presented in Fig. 5.

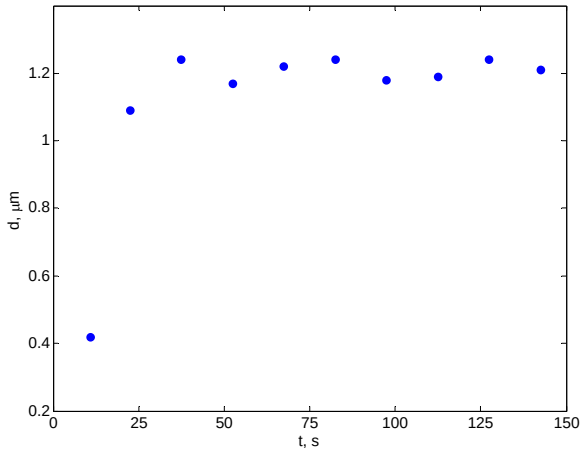

Fig. 5. The variation of the nanoparticle aggregates average diameter in time.

We should notice, however, that the diameter we measured using the procedure described above, which is basically a DLS using nontypical values for the experimental parameters and for the detection system, is the hydrodynamic diameter, which is slightly different of the physical diameter. Moreover, the presence of particles with a wide diameter distribution changes the shape of the PSD departing it from the theoretical shape, as presented in Fig. 4.

Examining Fig. 5 we notice a very fast increase of the average aggregate diameter in time. Actually after 22.5 seconds since the dilution was initiated we can no longer consider nanoparticles in suspension as the average measured diameter was bigger than 1 μm. As time passed the average diameter increasing rate decreased and a plateau can be noticed after 40 seconds. The average aggregate diameter remained around 1 μm; the variation around the average plateau value might be an artefact of the fitting procedure.

4. Discussion

In order to understand the significance of the average diameter previously mentioned and the variation of the average diameter in time, we should keep in mind that for small particles, comparable with the wavelength, Rayleigh approximation can be used to describe light scattering [39]. As the particle diameter d increases, at constant volume ratio, the nanoparticle number N should vary with the diameter d as:

$$N = \frac{V_{nano}}{\frac{4\pi}{3}\cdot\left(\frac{d}{2}\right)^3} \tag{4}$$

where V_{nano} is the total nanoparticle volume in suspension, a constant value. As light scattering on nanoparticles is a Rayleigh type scattering, the light intensity scattered by one individual particle is proportional to d^6 [39]. The average intensity scattered by all the nanoparticles in the sample and recorded at a constant angle is therefore proportional to d^3, thus increasing with the nanoparticle cluster diameter, as revealed by eq. (5).

$$< I > \approx N \cdot < I(\theta) > \approx \left(\frac{d}{2}\right)^3 \tag{5}$$

We notice from (5) that the light intensity scattered by one cluster having a diameter in the range of microns is roughly 10^6 bigger that the intensity scattered by one nanoparticle having a diameter around 10 nm, therefore the far field landscape becomes dominated by light scattered by clusters, as soon as they appear.

The average diameter calculated using the procedure described in the previous section is actually the scattering parameter of light scattered by clusters, therefore the average diameter is different from the average that can be calculated using TEM on a thin emulsion prepared from the nanofluid. Consequently the procedure described above is not sensitive in respect of measuring the amount of nanoparticles that turned into aggregates, but to reveal the presence of aggregates and to estimate the aggregation rate and the aggregates size.

Nevertheless, the experiment reveals that the procedure can be used for a half quantitative assessment of the time elapsed from the beginning of the dilution to the moment when cluster formation is completed in an aqueous suspension. Examining the results presented in Fig. 5 we notice that during the first 15 seconds a significant amount of nanoparticles turned into aggregates and the aggregate dimension was growing. After 20

seconds the aggregates dimension reached a plateau, which was found to be 1.2 μm by the modified DLS.

Another detail regarding the DLS technique is that the dynamic information of the particles is derived from an autocorrelation of the intensity trace recorded during the experiment. The modified version of the DLS uses the powerspectrum. Both of them decrease and the decrease rate depends, at constant angle and wavelength, of the diffusion coefficient of the particles in suspension, which, on it's turn depends of the rheological properties of the base fluid and of the diameter of the particles in suspension. Therefore DLS provides information on the hydrodynamic diameter of the particles, not on the physical diameter which is measured using TEM and other techniques.

5. Conclusions

In this work a simple experimental procedure, assisted by a set of computer programs required to process data is presented. The procedure consists of recording either a time series containing light scattered at small angles by suspensions over a time interval since the dilution process is initiated. The powerspectrum is computed and the diameter of the scattering centers is derived from a lest squares fit. The time variation of the average diameter of the aggregates in suspension is the output.

Using this procedure we found that magnetite nanoparticles having citric acid as surfactant, in aqueous diluted suspension, 0.17% volume ratio, aggregate very fast. During the first 20 seconds the aggregates dimension increases and the size reached a diameter bigger than 1.0 μm and this is extremely important when considering the nanoparticles for biomedical applications.

References

[1] P. Vadasz, J. Heat Transfer. **128**, 465 (2006).
[2] U. S. Choi, ASME Fed. **23**1, 99 (1995).
[3] S. P. Jang, S. U. S. Choi, Appl. Phys. Lett. **84**, 4316 (2004).
[4] W. Evans, J. Fish, P. Keblinski, Appl. Phys. Lett. **88**, 093116 (2006).
[5] Y. M. Xuan, W. Roetzel, Int. J. Heat Mass Transfer. **43**, 3701 (2000).
[6] R. Prasher, P. Brattacharya, P. E. Phelan, Phys. Rev. Lett. **94**, 025901 (2005).
[7] K. Butter , P. H. Bomans , P. M.Frederik, G. J. Vroege, A. P. Philipse, J. Phys.: Condens. Matter **15**, S1451S1451 (2003). doi: 10.1088/0953-8984/15/15/310.
[8] S. L. Tripp, S. V. Pusztay, A. E. Ribbe, A. Wei, J. Am. Chem. Soc. **124**, 7914 (2002).
[9] Z. Xiao, C. Cai, X. Deng, Chem. Commun. **1442–1443**, 2001. DOI: 10.1039/b104306b.
[10] S. B. Clendenning, S. F. Bidoz, A. Pietrangelo, G. Yang, S. Han, P. M. Brodersen, C. M. Yip, Z Lu, G. A. Ozin, I. Manners, J . Mater . Chem. **14**, 1686 (2004).
[11] O. V. Salata, Journal of Nanobiotechnology **2**, 3 (2004), doi:10.1186/1477-3155-2-3.
[12] Q. A. Pankhurst, J. Connolly, S. K. Jones, J. Dobson, J. Phys. D **36**, R167-R181 (2003).
[13] F. Zhang, S. W. Chan, J. E. Spanier, E. Apak, Q. Jin, R. D. Robinson, I. P. Herman, Appl. Phys. Lett. **80**, 27 (2002), doi:10.1063/1.1430502.
[14] L. M. Lacava, B. M. Lacava, R. B. Azevedo, Z. G. M. Lacava, N. Buske, A. L. Tronconi, P. C. Morais, Journal of Magnetism and Magnetic Materials **225**(1-2), 79 (2001).
[15] A. W. Hull, J. Am. Chem. Soc. **41**(8), 1168 (1919), DOI: 10.1021/ja02229a003.
[16] A. L. Patterson, Phys. Rev. **56** (10), 978 (1939), doi:10.1103/PhysRev.56.978.
[17] D. Chicea, Coherent Light Scattering on Nanofluids – Computer Simulation Results, Applied Optics **47**(10), 1434 (2008).
[18] J.W. Goodman, Laser speckle and related phenomena **9** in series Topics in Applied Physics, J.C. Dainty, Ed., Springer-Verlag, Berlin, Heidelberg, New York, Tokyo, 1984.
[19] J. David Briers, Physiol. Meas. **22**, R35 (2001).
[20] M. Giglio, M. Carpineti, A. Vailati, D. Brogioli, Appl. Opt. **40**, 4036 (2001).
[21] Y. Piederrière, J. Cariou, Y. Guern, B. Le Jeune, G. Le Brun, J. Lotrian, Optics Express **12**, 176 (2004).
[22] Y. Piederriere, J. Le Meur, J. Cariou, J.F. Abgrall, M.T. Blouch, Optics Express **12**, 4596 (2004).
[23] D. Chicea, European Physical Journal Applied Physics **40**, 305 (2007), DOI: 10.1051/epjap:2007163
[24] G. V. R. Born, J. Physiol. **209**, 487 (1970).
[25] Y. Ozaki, K. Satoh, Y. Yatomi, T. Yamamoto, Y. Shirasawa, S. Kume, Anal. Biochem. **218**, 284 (1994).
[26] K. Yabusaki, E. Kokufuta, Langmuir **18**, 39 (2002).
[27] Ioan Turcu, Silvia Neamtu, Cristian V. L. Pop, Int. Conf. on Isotopic Processes PIM5, 2007.
[28] I. V. Mindukshev, I. E. Jahatspanian, N. V. Goncharov, R. O. Jenkins, A. I. Krivchenk, Spectroscopy – Int. J. **19**, 235 (2005).
[29] I. V. Mindukshev, E. E. Ermolaeva, E. V. Vivulanets, E. Yu. Shabanova, N. N. Petrishchev, N. V. Goncharov, R. O. Jenkins, A. I. Krivchenko, Spectroscopy – Int. J. **19**, 247 (2005).
[30] D. Chicea, C. M. Goncea, On Magnetic Nanofluid Synthesis and Physical Properties, in press.
[31] W. Tscharnuter, in Encyclopedia of Analytical Chemistry, R. A. Meyers (ed), John Wiley & Sons Ltd, 5469, 2000.
[32] B. B. Weiner, Chapt. 5 in Liquid-and Surface-Borne Particle Measurement Handbook, J. Z. Knapp, T. A. Barber, A. Liebermann (ed), Marcel Dekker Inc. NY, 1996.
[33] N. A. Clark, J. H. Lunacek, G. B. Benedek, American Journal of Physics **38**(5), 575 (1970).
[34] S. B. Dubin, J. H. Lunacek, G. B. Benedek, PNAS **57**(5), 1164 (1967).
[35] Berne, Pecora, Dynamic Light scattering, John Wiley,

1975.
[36] J. W. Goodman, Statistical Optics, Wiley Classics Library Edition, 2000.
[37] E. Hecht, Optics, Addison-Wesley, New York, 2001.
[38] J. D. Briers, Physiol. Meas. **22**, R35 (2001).
[39] C. F. Bohren, D. Huffman, Absorption and scattering of light by small particles, John Wiley, New York, 1983.

*Corresponding author: dan.chicea@ulbsibiu.ro